Zhijie Wang
Department of Biomedical Engineering,
University of Wisconsin,
2146 ECB, 1550 Engineering Drive,
Madison, WI 53706

Jasmin Kristianto
Geriatrics Research, Education,
and Clinical Center,
William S. Middleton Veterans Hospital,
2500 Overlook Terrace,
Madison, WI 53705;
Division of Endocrinology,
Department of Medicine,
University of Wisconsin,
4148 MFCB (5148), 1685 Highland Avenue,
Madison, WI 53705;
Endocrine and Reproductive Physiology Program,
University of Wisconsin,
1465 MSC, 1300 University Avenue,
Madison, WI 53706

Chen Yen Ooi[1]
Department of Biomedical Engineering,
University of Wisconsin,
2146 ECB, 1550 Engineering Drive,
Madison, WI 53706

Michael G. Johnson

Suzanne J. Litscher

Thomas D. Pugh

Gurpreet Sandhu[2]

Geriatrics Research, Education,
and Clinical Center,
William S. Middleton Veterans Hospital,
2500 Overlook Terrace,
Madison, WI 53705;
Division of Endocrinology,
Department of Medicine,
University of Wisconsin,
4148 MFCB (5148), 1685 Highland Avenue,
Madison, WI 53705

Naomi C. Chesler
Department of Biomedical Engineering,
University of Wisconsin,
2146 ECB, 1550 Engineering Drive,
Madison, WI 53706

Robert D. Blank[3]
Geriatrics Research, Education,
and Clinical Center,
William S. Middleton Veterans Hospital,
2500 Overlook Terrace,
Madison, WI 53705;
Division of Endocrinology,
Department of Medicine,
University of Wisconsin,
4148 MFCB (5148), 1685 Highland Avenue,
Madison, WI 53705;
Endocrine and Reproductive Physiology Program,
University of Wisconsin,
1465 MSC, 1300 University Avenue,
Madison, WI 53706
e-mail: rdb@medicine.wisc.edu

Blood Pressure, Artery Size, and Artery Compliance Parallel Bone Size and Strength in Mice With Differing Ece1 Expression

The recombinant congenic mouse strains HcB-8 and HcB-23 differ in femoral shape, size, and strength, with HcB-8 femora being more gracile, more cylindrical, weaker, and having higher Young's modulus. In previous work, we mapped a robust, pleiotropic quantitative trait locus for these bone traits. Ece1, encoding endothelin converting enzyme 1, is a positional candidate gene for this locus, and was less expressed in HcB-8 bone. We hypothesized that the same genetic factors would impose analogous developmental trajectories on arteries to those in bones. Cardiovascular hemodynamics and biomechanics of carotids were measured in adult HcB-8 and HcB-23 mice. Biological differences in heart and arteries were examined at mRNA and protein levels. As in bone, Ece1 expression was higher in HcB-23 heart and arteries ($p < 0.05$), and its expression was correlated with that of the endothelin B type receptor target Nos3, encoding endothelial nitric oxide synthase. HcB-8 mice had higher ambulatory blood pressure ($p < 0.005$) than HcB-23 mice. Ex vivo, at identical pressures, HcB-8 carotid arteries had smaller diameters and lower compliance ($p < 0.05$), but the same elastic modulus compared to HcB-23 carotid arteries. HcB-8 hearts were heavier than HcB-23 hearts ($p < 0.01$). HcB-8 has both small, stiff bones and small, stiff arteries, lower expression of Ece1 and Nos3, associated in each case with less favorable function. These findings suggest that endothelin signaling could serve as a nexus for the convergence of skeletal and vascular modeling, providing a potential mechanism for the epidemiologic association between skeletal fragility and atherosclerosis. [DOI: 10.1115/1.4024161]

Keywords: blood pressure, arterial modeling, endothelin converting enzyme 1, nitric oxide synthase 3, recombinant congenic mice

Introduction

Mechanical loading of bone induces strain, leading to modeling or remodeling of bone to maintain homeostasis within the physiological strain range [1]. Shear stress arising from fluid flow within bone's canalicular system and sensed by osteocytes is thought to be the operative stimulus [2]. Similar adaptations are found in

[1]Present address: Bioengineering Office, Department of Engineering, University of Cambridge, Trumpington Street, Cambridge, CB2 1PZ, UK.
[2]Present address: Faculty of Medicine, St. Martinus University, Brionplein 1, Otrobanda, P.O. Box 2050, Curaçao.
[3]Corresponding author.
Contributed by the Bioengineering Division of ASME for publication in the Journal of Biomechanical Engineering. Manuscript received June 26, 2012; final manuscript received December 21, 2012; accepted manuscript posted April 8, 2013; published online May 9, 2013. Assoc. Editor: Hai-Chao Han.

vascular tissues, where arteries remodel in response to fluid shear stress and pressure to maintain wall shear stress and intramural wall stress within physiological limits [3]. The potent vasodilator nitric oxide (NO) is known to play a role both in skeletal load-induced modeling [4] and mechanotransduction in blood vessels [5]. Induction of NO synthesis by endothelial nitric oxide synthase (NOS3 or eNOS) is a central feature of both bone [6–8] and arterial [5] mechanostransduction.

An epidemiological association between osteoporosis and atherosclerosis has been reported by multiple research groups [9–11], suggesting that shared mechanisms might exist in the physiological conditions and pathogenesis of skeletal and vascular tissues. Several studies have identified pathways contributing to such correlations [12,13]. In spite of these findings, the biology underlying the association remains incompletely understood.

We have studied the genetics underlying bone's biomechanical performance in the recombinant congenic mouse strains HcB-8 and HcB-23, each of which derives ~1/8 of its genome from C57BL/10ScSnA and the remainder from C3H/DiSnA [14]. Thus, HcB-8 and HcB-23 harbor different alleles at about one-fourth of the differential loci between the progenitor strains. Consequently, HcB-8 and HcB-23 bones differ substantially in the architecture and biomechanical performance of their femora, and we identified quantitative trait loci (QTLs) for multiple structural and biomechanical features of the femur and the mandible [15–18]. In brief, HcB-23 bones are larger and more elliptical in cross-section, stronger, and have higher bone mineral density than HcB-8 bones. HcB-8 bones, however, have greater ductility and Young's modulus than HcB-23 bones. These structural and mechanical properties are robust predictors of low trauma fracture and thus may be considered "osteoporotic."

Ece1, encoding endothelin converting enzyme 1, is a positional candidate for the most robust and pleiotropic QTL. ECE1 is a membrane-bound bound, zinc-dependent endopeptidase that catalyzes the cleavage of the biologically inert, 34 amino acid "big endothelin" to the active, 21 amino acid endothelin 1 (ET-1) [19,20]. *Nos3* is also known to be induced by endothelin signaling via the endothelin B type receptor (EDNRB) [21,22]. Notably, both HcB-8 and HcB-23 harbor the same *Nos3* allele, so that differences in its expression in adult tissues reflect differences in physiological regulation, rather than an inherent difference in *Nos3* transcriptional activity.

Here, we sought to determine whether hemodynamic and vascular biomechanical performance differ between HcB-8 and HcB-23 arteries, due to the potential shared endothelin-NO pathway. We hypothesized that the genetic factors driving strain-specific modeling in bones would act similarly in arteries, resulting in differences in compliance and geometry between the HcB-8 and HcB-23 arteries. We compared systemic hemodynamics and carotid geometrical and mechanical properties between the HcB-8 and HcB-23 mouse strains. We found that HcB-8 mice had markedly higher ambulatory blood pressure (BP) and more massive hearts than HcB-23 mice, with smaller and less compliant arteries. Furthermore, *Ece1* expression differed between the strains, and correlated with *Nos3* expression.

Methods

Animal Husbandry. HcB-8 and HcB-23 mice were maintained as described previously [15]. Animals used for tissue isolation were euthanized by CO_2 asphyxiation; animals used for hemodynamic measurements were euthanized by cervical dislocation. All procedures conformed to the NIH Guide for the Care and Use of Laboratory Animals and were approved by the William S. Middleton Veterans Hospital and the University of Wisconsin IACUCs.

***In Vivo* Hemodynamics.** Unanesthetized male mice underwent ambulatory BP and heart rate measurement by volume pulse recording of the tail (Coda 2, Kent Scientific, Torrington, CT). Animals were trained for one week prior to beginning the study. Measurements were repeated 20–30 times per session, and averaged to give the daily average for each animal.

Four to 6 month old male mice were anesthetized with isoflurane (1.5–2.5%), intubated, and placed on a ventilator (Harvard Apparatus, Holliston, MA). The right common carotid artery was isolated and a 1.4 Fr high-fidelity pressure catheter (Millar Instruments, Houston, Texas) was inserted and advanced to the aorta. The aortic pressures and heart rate were recorded and analyzed on commercially available software (Notocord, Croissy Sur Seine, France). Blood velocity and inner diameter of the carotids were measured using a Vevo 770 ultrasound (Visual Sonics) 30 MHz probe, following the leading edge to leading edge convention.

Arterial Biomechanics. After euthanasia (by CO_2 asphyxiation), left common carotid arteries were harvested for mechanical testing. Care was taken to avoid vessel collapse during harvest and mounting in the isolated vessel testing system.

The mechanical testing system was set up as previously reported [23]. The left carotid arteries were mounted with sutures on 340 μm-diameter cannulas in a vessel chamber (Living System Instrumentation (LSI), Burlington, VT). A servo-control pump (LSI) was used to apply steady intramural pressure by perfusion of Dulbecco's phosphate buffered saline solution (PBS, without calcium and magnesium, MP Biomedicals, Solon, OH). Two pressure transducers (P1 and P2) were placed next to the cannulas on both sides of the vessel to obtain the average pressure ($P = (P1 + P2)/2$). Images of the vessels were captured with a CCD camera (IonOptix, Milton, MA) connected to an inverted microscope (Olympus, Center Valley, PA) at 10× magnification, and sent to a video dimension analyzer (VDA, LSI) for automatic detection of outer diameter (D_o) along a single line at the approximate middle, length-wise, of the vessel. The vessel bath was maintained at 37 °C and *p*H 7.4 by continuous perfusion of *p*H-adjusted Dulbecco's PBS using a superfusate pump (Ismatec, Glattbrugg, Switzerland).

After mounting, the unstretched lengths of the vessels were measured from suture to suture. They were then stretched 150% to prevent buckling at higher pressures. Cannula ends were held fixed so that the vessel length remained constant throughout the test. Vessels were allowed to equilibrate at 90 mm Hg for 30 min, followed by wall thickness (h) measurements at transmural pressures of 5, 90, and 120 mm Hg, and another 30-min equilibrium. Next, vessels were preconditioned with five sinusoidal pressurization cycles from 90 to 120 mm Hg at 0.014 Hz. After resting at 5 mm Hg for 1 min, pressure steps from 90 to 120 mm Hg were applied at 5 mm Hg increments for 1 min at each step. Pressure and D_o were sampled at 1 Hz through LABVIEW (National Instruments (NI), Austin, TX), sent to a data acquisition system (DAQ) (NI), and recorded. Data at the end of each pressure step were used for the passive mechanical property calculations.

***In Vivo* and *Ex Vivo* Length Measurement.** *In vivo* left common carotid artery length was measured *in situ* from its origin at aortic arch to the branch of internal and external carotids. The distance between these landmarks was then measured after vessel harvest to obtain the *ex vivo* length. For each mouse, the ratio of the *in vivo* length to the *ex vivo* length, or axial stretch ratio, was obtained.

Opening Angle Measurement. To examine the arterial zero-stress state, left carotid arteries were harvested and cut into 1–2 mm ring segments perpendicular to the arterial axis and then cut open radially. The rings were placed in PBS for ~30 min at 37 °C to fully release the residual stress [24]. Rings were imaged on an inverted microscope (Micromaster, Thermo Fisher Scientific Inc., Waltham, MA), and captured using MICRON v2.0 software (Westover Scientific, Mill Creek, WA). The opening angle

was measured as the angle between two lines originating from the midpoint to tips of inner wall [24] using IMAGEJ (NIH).

Hemodynamics and Biomechanics Calculations. From the anesthetized *in vivo* hemodynamic measurements, carotid artery wall shear stress (WSS) was calculated as previously reported [25]:

$$\mathrm{WSS} = \frac{4 \times \mu \times V}{D_i} \tag{1}$$

where μ is the blood viscosity (assumed to be 0.035 dyn-s/cm^2), and V and D_i are the mean blood velocity and inner diameter of the carotid artery, respectively.

For isolated vessel passive mechanical testing, pressure–outer diameter (P–D_o) relationships were obtained in the pressure range of 90–120 mm Hg to calculate arterial mechanical properties. Arteries were assumed to be homogeneous and incompressible [26–28]. Wall thickness (h) as a function of pressure was calculated assuming conservation of mass as

$$h = \frac{1}{2}\left(OD - \sqrt{OD^2 - OD_{90}^2 + (OD_{90} - 2h_{90})^2}\right) \tag{2}$$

where D_{o90} and h_{90} are the D_o and h measured optically *ex vivo* at 90 mm Hg, respectively. The overall stiffness was examined by calculating circumferential stretch (λ) and compliance (C) as functions of pressure

$$\lambda = \frac{\pi \times D_o}{\pi \times D_{o5}} = \frac{D_o}{D_{o5}} \tag{3}$$

$$C = \frac{\Delta A_i}{\Delta P} \tag{4}$$

where D_{o5} is the D_o at 5 mm Hg to approximate no-load state, as done previously [23,27], and ΔA_i is the change of luminal cross-sectional area for a step pressure change (ΔP) of 5 mm Hg calculated between 90 and 120 mm Hg. We use D_o at 5 mm Hg as no-load reference because in our prior studies pressures less than 5 mm Hg occasionally led to vessel collapse, which not only precludes diameter measurement at that pressure, but also can damage the endothelium. Carotid artery material behavior was further investigated with the stress-strain relationship and the elastic modulus (E) derived from the stress-strain curve. The midwall circumferential stress (σ) and strain (ε) were calculated using thin-walled assumption and Green's formulation for finite deformation

$$\sigma = \frac{P \times D_m}{2h} \tag{5}$$

$$\varepsilon = \frac{1}{2}\left(\frac{D_m^2}{D_{m5}^2} - 1\right) \tag{6}$$

where D_m is the midwall diameter and D_{m5} is the mid-wall diameter at 5 mm Hg. Midwall stress and strain were chosen so that the no-load state could be used as the reference state instead of the zero-stress state [29]. E was obtained as the slope of the line fit to the stress-strain curves to measure the material stiffness of the vessel. Nonlinear measures were not used because the stress-strain behavior of the arteries in this small, physiological pressure range (90–120 mm Hg) was fairly linear; the average linear correlation coefficient (R^2) was 0.98.

Protein Content, Immunohistochemistry, and mRNA Levels. To measure collagen content, carotids were harvested and flash frozen. Tissue homogenates were assayed for hydroxyproline (OHP) content as a marker for collagen content, using standard techniques [30]. The total tissue OHP content is presented as μg/vessel.

Rabbit polyclonal IgG against ECE1 (SC-25841), NOS3 (SC-654), PECAM1 (SC-28188), and goat polyclonal IgG against DMP1 (SC-6551) were purchased from Santa Cruz Biotechnology (Santa Cruz, CA). We used dilutions of 1:200, 1:200, and 1:1000, respectively for primary antibody binding. We used biotinylated goat anti-rabbit IgG (BA1000) and biotinylated rabbit anti-goat

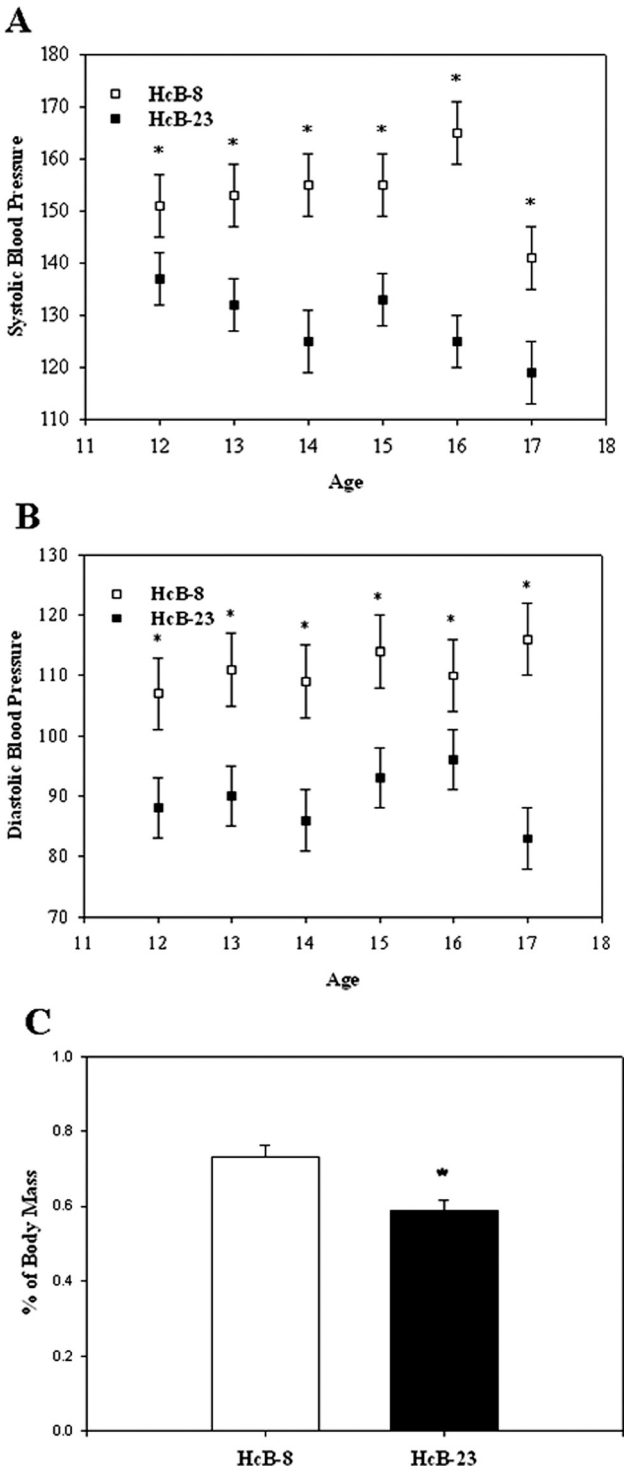

Fig. 1 Ambulatory BP and heart size. The difference in (*a*) systolic ($p = 0.002$), (*b*) diastolic ($p < 0.001$) BP, and (*c*) normalized heart mass ($p < 0.01$) between HcB-8 and HcB-23 is significant. N = 8 for HcB-8 and 10 for HcB-23. * $p < 0.05$.

Table 1 Anesthetized hemodynamics[a] and *ex vivo* biomechanics[b]

Parameters	HcB-8	HcB-23
Heart rate (bpm)	415 ± 17	391 ± 9
Blood velocity (mm/s)	304 ± 41 ($n = 4$)	285 ± 43 ($n = 3$)
Wall shear stress (dyne/cm^2)	87 ± 17 ($n = 4$)	78 ± 10 ($n = 3$)
Systolic pressure (mm Hg)	89 ± 6	88 ± 12
Diastolic pressure (mm Hg)	68 ± 5	68 ± 10
Mean pressure (mm Hg)	77 ± 5	77 ± 11
Outer diameter (D_{o5}) at 5 mm Hg (μm)	356 ± 25	380 ± 16[c]
Outer diameter (D_{o90}) at 90 mm Hg (μm)	556 ± 13	601 ± 10
Wall thickness (h) at 90 mm Hg (μm)	39 ± 1	36 ± 2
E from 90 to 120 mm Hg (kPa)	287 ± 16	269 ± 29
Opening Angle (OA) in degrees	23 ± 4 ($n = 5$)	68 ± 14[c] ($n = 6$)
Ex vivo Length (mm)	4.5 ± 0.2 ($n = 5$)	5.7 ± 0.3[c] ($n = 6$)
Axial stretch ratio	2.0 ± 0.0 ($n = 5$)	1.7 ± 0.1[c] ($n = 6$)
Hydroxyproline content (μg/vessel)	4.0 ± 0.6 ($n = 5$)	7.1 ± 0.7[c] ($n = 6$)

[a]For anesthetized hemotynamics $n = 7$/strain, except where noted otherwise.
[b]For *ex vivo* biomechanics $n = 10$, except where noted otherwise.
[c]Significant difference from HcB-8 at $p < 0.05$.

IgG (BA5000) from Vector Laboratories (Burlingame, CA) at a concentration of 7.5 μg/ml as secondary antibodies. For the heart histology, horseradish peroxidase activity was used to visualize antibody binding with the Vectastain ABC and Peroxidase Nova Red kits (PK6100 and SK4800, Vector Laboratories), as recommended by the manufacturer. For the carotid artery histology, Vectastain ABC and DAB peroxidase substrate kit, 3, 3'-diaminobenzidine (PK6100 and SK-4100, Vector Laboratories) were used as recommended by the manufacturer to visualize the antibody binding.

All western blot reagents were purchased from Santa Cruz Biotechnology (Santa Cruz, CA) unless stated otherwise. For western blotting, we examined the protein levels of ECE1 and NOS3 in arteries using femoral arteries because of the limited amount of carotid artery tissue. The femoral arteries and heart tissue samples were homogenized (100 mM Tris, *p*H 7.4, 20% sucrose, 0.1 M phenylmethylsulfonyl fluoride (CAS-329-98-6), and 1 μg/ml Leupeptin (SC-3141)). Protein concentrations of the femoral arteries, heart and bone tissue samples were measured via Bradford assay. The cell lysates were subjected to 10% Mini Protean TGX precast gels (BioRad) and transferred to PVDF plus membrane (Osmonics Inc, Minnetonka, MN). ECE1 and NOS3 expression was detected using rabbit polyclonal IgG against ECE1 (SC-25841) and NOS3 (SC-654). We used dilutions of 1:200 for both primary antibodies. The blots were washed and incubated with goat anti rabbit IgG-HRP (SC-2004) at 1:1000 dilution and developed using ECL (Amersham, Piscataway, NJ).

Messenger RNA levels in hearts were measured by the ΔC_t method, using ribosomal protein L32 as a reference [31]. Analyses were performed in a StepOne RT-PCR instrument (Applied Biosystems, Carlsbad, CA), using TaqMan (Applied Biosystems) assay kits according to the manufacturer's instructions.

Statistics. Results are presented as mean ± SEM. The association between vessel stretch and mouse strain was analyzed using a linear mixed effect model with repeated measures. Differences in ambulatory and anesthetized invasive hemodynamics, *in vivo* and *ex vivo* geometry, mRNA and protein expressions in tissues, and *ex vivo* mechanical and material properties were analyzed by unpaired t-test or repeated measures ANOVA. Analyses were performed using R[4] version 2.5.1 or SIGMASTAT 3.0 (Systat, San Jose, CA); $p < 0.05$ was considered significant.

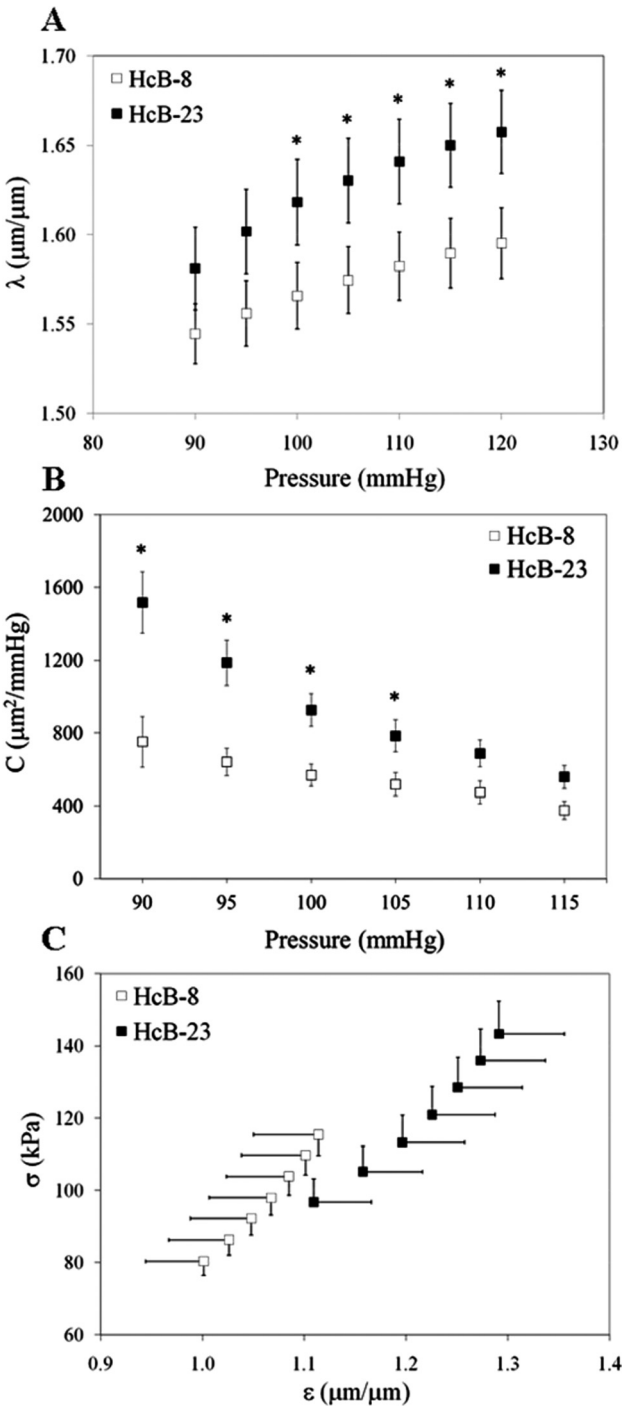

Fig. 2 Carotid artery mechanical properties. (*a*) Stretch (λ) as a function of transmural pressure. (*b*) Compliance (*c*) as a function of transmural pressure. (*c*) Circumferential stress versus Green's strain (σ–ε) obtained from 90 to 120 mm Hg. * $p < 0.05$. N = 10 for HcB-8 and N = 8 for HcB-23.

Results

***In Vivo* Hemodynamics.** While average heart rate did not differ (653 ± 15 bpm for HcB-8 *v* 676 ± 11 bpm for HcB-23, NS), BP was consistently higher in awake HcB-8 mice than HcB-23

[4]See R-project.org

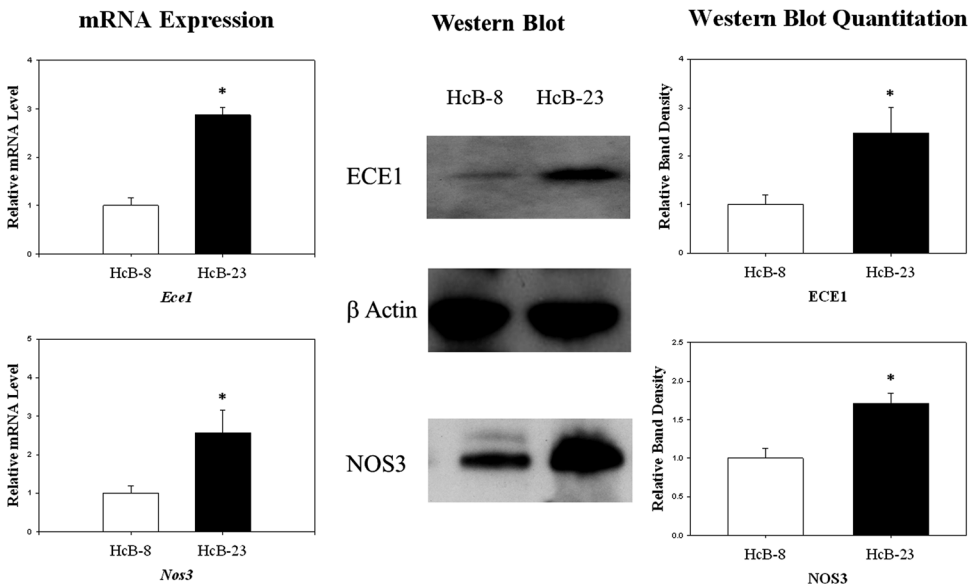

Fig. 3 Expression levels of Ece1 and Nos3 in heart. Top, Ece1 mRNA ($p < 0.001$), Ece1 protein ($p = 0.04$). Bottom. Nos3 mRNA ($p = 0.04$), Nos3 protein ($p = 0.008$). * $p < 0.05$. N = 4/strain for all comparisons.

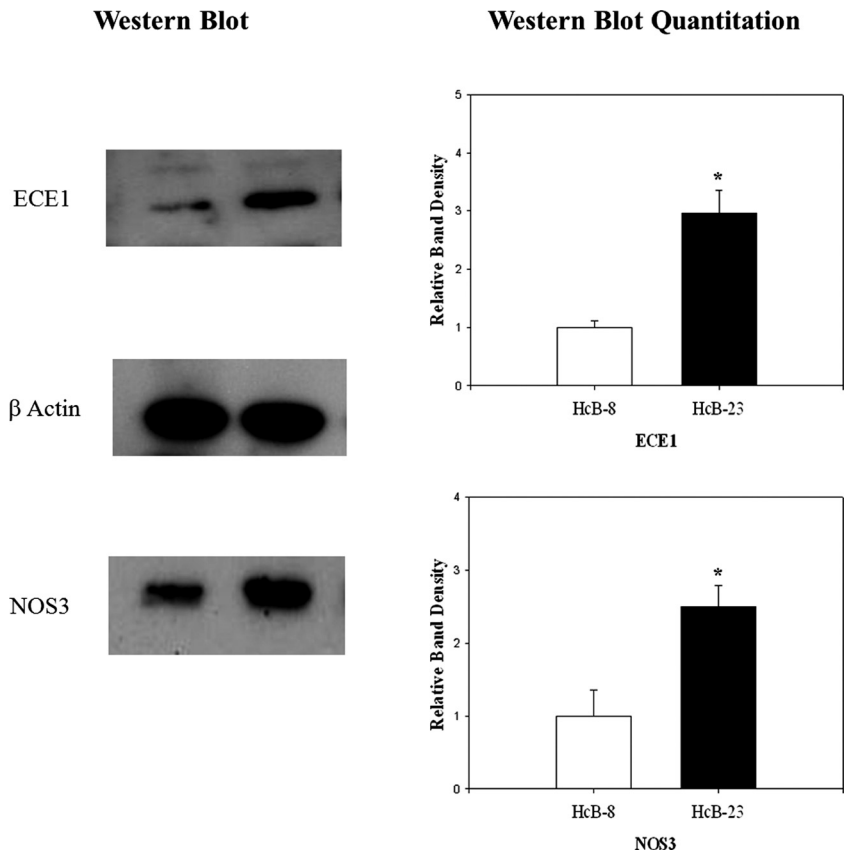

Fig. 4 Expression levels of Ece1 and Nos3 in femoral artery. Relative Ece1 ($p = 0.001$, N = 5/strain) and Nos3 ($p = 0.01$, N = 5/strain) protein levels are higher in HcB-23 mice. * $p < 0.05$

mice (Figs. 1(*a*) and 1(*b*)). We did not observe any difference in pulse pressure (= systolic BP – diastolic BP) between the two strains (36 ± 3 mm Hg for HcB-8 *v* 35 ± 4 mm Hg for HcB-23, NS). Hearts harvested at 17 weeks of age were more massive in the HcB-8 mice (Fig. 1(*c*)).

Hemodynamic parameters were also measured in anesthetized animals. At these lower heart rates (Table 1), there were no differences in aortic BP. Also, there were no differences in carotid artery blood velocity or carotid artery wall shear stress (WSS), although both tended to be lower in HcB-23 mice.

Arterial Biomechanics. HcB-23 arteries had longer *ex vivo* lengths than HcB-8 arteries, but the *in vivo* lengths were not different (Table 1). Consequently, the axial stretch ratio was larger in HcB-8 arteries (Table 1). The opening angle of HcB-23 carotids was larger than that of HcB-8 carotids (Table 1).

Carotid artery outer diameter and wall thickness were measured in the isolated vessel testing system to quantify the impact of genetics on arterial morphometry. At transmural pressures of 5 and 90 mm Hg, the outer diameters of HcB-23 arteries were larger than HcB-8 arteries ($p < 0.05$), whereas wall thickness was similar (Table 1).

Circumferential stretch (λ) and compliance (C) of the carotid arteries were computed to measure overall stiffness. HcB-23 arteries stretched more and had higher compliance than HcB-8 arteries at pressures $\leq$110 mm Hg (Figs. 2(*a*) and 2(*b*)). As pressure increased, the compliance of HcB-23 carotids declined more rapidly than that of the HcB-8 carotids, eliminating the compliance difference at higher pressures.

Stress-strain (σ–ε) curves and elastic moduli (E) were calculated to investigate the material properties of HcB-8 and HcB-23 carotid arteries. From 90 to 120 mm Hg, the HcB-23 carotids operated in a higher stress and strain range (Fig. 2(*c*)). However, E calculated from the stress-strain curves were not different (Table 1). Therefore, these data suggest that the difference in the overall stiffness is largely a consequence of the difference in geometry (i.e., vessel size).

Protein Content, Expression and mRNA Levels. Since a major quantitative trait locus for bone size, shape, and mechanical performance maps to the chromosome region harboring *Ece1*, we measured the mRNA and/or protein expression levels of *Ece1* and the downstream molecule *Nos3* in heart, carotid, and femoral arteries.

In heart, *Ece1* mRNA was ~3-fold and ECE1 protein was ~2.5-fold more highly expressed in HcB-23 mice, while *Nos3* mRNA was ~2.5-fold and NOS3 protein was ~1.7-fold more abundant in HcB-23 mice (Fig. 3). In femoral arteries, ECE1 protein was threefold and NOS3 protein was ~2.fivefold more abundant in HcB-23 mice (Fig. 4). We did not measure mRNA expression in femoral arteries due to the limited available tissues. These differences in protein and mRNA expression between the mouse strains were also observed in bone. We found *Ece1* mRNA and *Ece1* protein were both ~1.6-fold more highly expressed in HcB-23 bones ($p < 0.05$, data not shown).

Immunohistochemistry of the heart and carotid artery further confirmed the differences in the protein levels as shown above. HcB-23 hearts contain substantially more ECE1 (Figs. 5(*a*) and 5(*b*)), and moderately more NOS3 than HcB-8 hearts (Figs. 5(*c*) and 5(*d*)). The same disparity in ECE1 and NOS3 content was also apparent in carotid arteries (Figs. 5(*g*)–5(*j*)). PECAM1 stains arteries from both strains equivalently (Figs. 5(*e*) and 5(*f*)), suggesting that endothelium is intact.

To investigate the underlying mechanisms for the differences in arterial biomechanics between HcB-8 and HcB-23 strains, we also examined the collagen content of the carotid arteries and found it was greater in HcB-23 than in HcB-8 mice (Table 1). To eliminate the effect of vessel size on the collagen content, we estimated the relative collagen content by normalizing by average vessel volume measured from ultrasound in different groups of mice. The result showed the same trend: HcB-23 carotid arteries have more collagen on average than HcB-8 carotid arteries (data not shown).

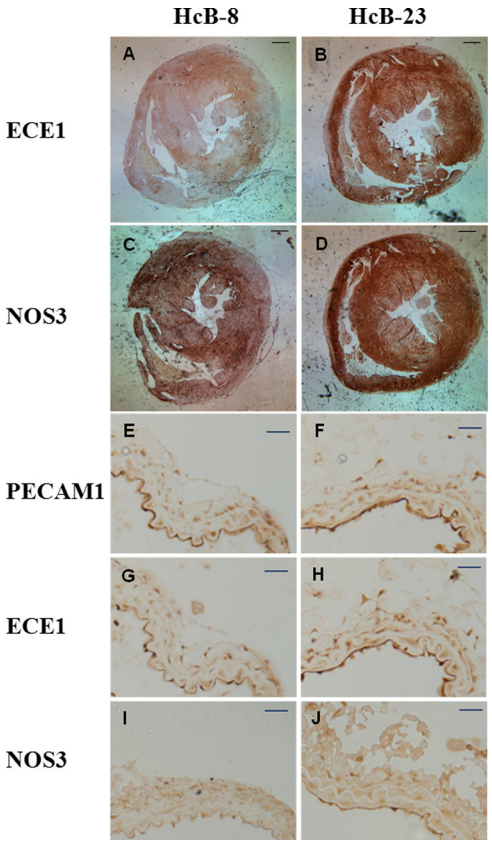

Fig. 5 Immunohistochemistry of hearts and carotid arteries. Heart (*a*)–(*d*) and carotid artery (*e*)–(*h*) stained as indicated. Ece1 (*a*), (*b*), (*g*), (*h*), Nos3 (*c*), (*d*), (*i*), (*j*), and PECAM1 (*e*), (*f*). HcB-8 (*a*), (*c*), (*e*), (*g*), (*i*), HcB-23 (*b*), (*d*), (*f*), (*h*), (*j*). Scale bars are 1 mm for heart sections and 50 μm for carotid artery sections.

Discussion

We previously mapped a robust, pleiotropic QTL for femoral size, shape, and biomechanical performance to a short region of chromosome 4 harboring *Ece1* [15–18]. Femora of mice harboring HcB-23 allele are larger, stronger, and more brittle than those harboring the HcB-8 allele, implying an involvement of endothelin pathways in bone modeling. Because the endothelin system has multiple important roles in the development and physiology of the vascular system, we undertook experiments to determine whether parallel phenotypic differences exist in arteries. The experiments summarized here demonstrate that HcB-8 and HcB-23 differ in *Ece1* expression in heart and arteries and that the expression difference is associated with differences of ambulatory blood pressure, normalized heart weight, arterial size and mechanical properties, and expression of *Nos3*.

In particular, the data presented here demonstrate that decreased expression of *Ece1* in HcB-8 mice is associated with lesser arterial size (outer diameter) and greater arterial stiffness. Functionally, lower *Ece1* expression is associated with higher ambulatory BP and greater heart weight, suggesting that the sustained ambulatory BP difference may contribute to cardiac hypertrophy. Whereas the smaller diameter of HcB-8 arteries resulted in an overall lower circumferential stress and strain range than HcB-23 arteries over the same pressure range, because the ambulatory pressures are higher in the HcB-8 strain, the physiological stress and strain ranges are the same. As a consequence of the diameter difference, however, at each applied pressure, the smaller HcB-8 arteries are stiffer than the larger HcB-23 arteries. Since neither wall thickness nor elastic modulus differs between the strains, the luminal diameter of the vessel is the key factor in the difference in overall carotid stiffness between the two mouse strains. Analogously, radius is a major determinant of bone strength and stiffness [32].

While we did not find a difference in WSS in the anesthetized state, one likely exists in the waking state. At ambulatory diastolic pressures specific to each strain (~90 mm Hg for HcB-23 and

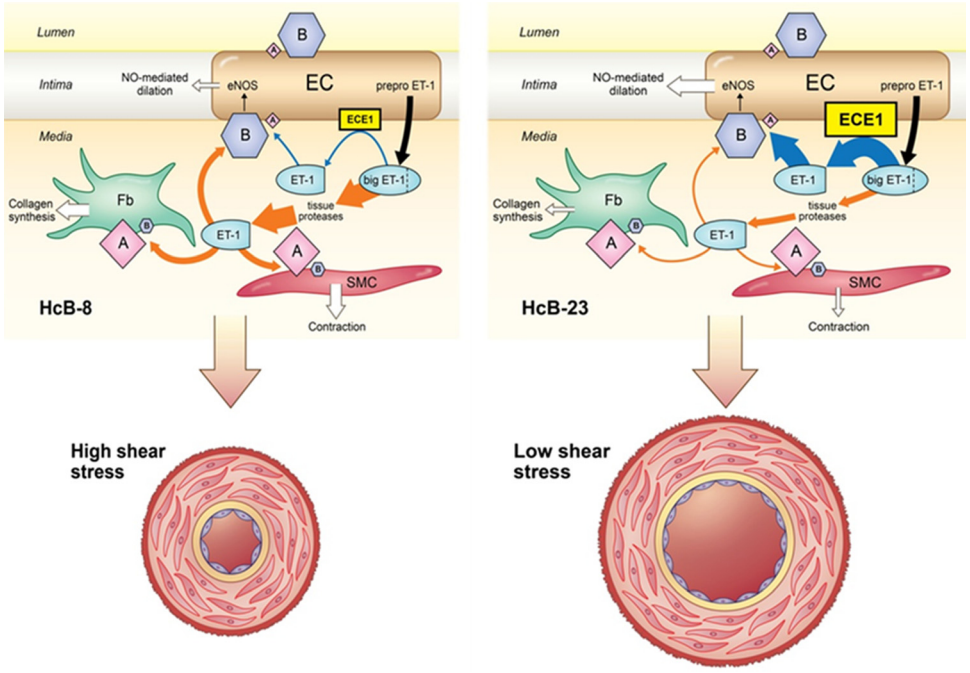

Fig. 6 Schematic of ET-1 signaling in HcB-8 and HcB-23 arteries. HcB-8 arteries (left) have low Ece1 expression. Big ET-1 is cleaved to active ET-1 primarily by tissue proteases and signaling SMC preferentially. A is the predominant receptor type in these cells, with its activation favoring SMC contraction and development of narrow, stiff vessels. HcB-23 arteries (right) have high Ece1 expression. Big ET-1 is cleaved to active ET-1 primarily by Ece1, signaling EC preferentially. B is the predominant receptor type in these cells, with its activation favoring NO production and development of wide, compliant vessels. A = A type ET-1 receptor. B = B type ET-1 receptor. EC = endothelial cell. SMC = smooth muscle cells. Sizes of symbols and arrows represent abundance of proteins and activity of pathways, respectively.

~110 mm Hg in HcB-8) the circumferential stretch is similar (~1.58). Since the HcB-23 carotids are larger at 5 mm Hg, the diameters will remain proportionately larger than HcB-8 at their *in vivo* pressures. Thus, for the same volumetric flow rate, the HcB-23 WSS should be smaller.

Integrating these potential hemodynamic differences and the evidence found here of biological differences between the strains, we speculate that *Ece1* activity and expression modulate artery growth and modeling as shown in Fig. 6. Our data suggest that in HcB-8 mice, the low endothelial *Ece1* activity may direct ET-1 signaling preferentially toward smooth muscle cells, with limited endothelial NO synthesis. This combination of factors might lead to increased smooth muscle tone and thus smaller artery diameter. In contrast, high endothelial *Ece1* activity in HcB-23 mice may potentially direct ET-1 signaling preferentially to endothelial cells. This would then induce *Nos3*, NO production, smooth muscle cell relaxation, and thus a larger arterial diameter. We speculate that endothelial cell function is impaired to some degree in HcB-8 mice, which are unable to produce enough NO to dilate and outwardly remodel the arterial lumen. This suggestion, coupled with the mild hypertension, indicates that HcB-8 mice may be prone to atherosclerosis, much as their bones are most osteoporotic in phenotype.

Mechanical forces are known to be critical drivers of development in the vascular system. In chick embryos, shear stress induces *Nos3* expression and vascular remodeling in the yolk sac [33]. Furthermore, shear stress in intracardiac arteries during development causes localized *Ece1* expression, which in turn drives transdifferentiation of cardiomyocytes to Purkinje cells [34,35]. Modulating the mechanical environment alters the timing of Purkinje system development in the chick [34,35]. Transdifferentiation of cardiomyocytes can be induced in the absence of blood flow by ectopic expression of *Ece1* and *Edn1* [36]. After birth, arteries retain the ability to remodel in response to mechanical stimuli. In rat mesenteric arteries, luminal growth is mediated by shear stress and *Nos3* expression [37]. Moreover, the capacity of carotid arteries to remodel in response to partial ligation is genetically programmed in mice [38]. ET signaling is an important regulator of NO synthesis via *Nos3* induction. The regulation of ET-1 and NOS3 expression in endothelium is often reciprocal [20,39], but ET-1 and NO are not simple antagonists. ET-1 binding to EDNRB stimulates vasodilation through the NO production pathway [20,21]. These findings establish the importance of mechanical signals in establishing the diameter of blood vessels and transduction of mechanical stimuli via endothelin signaling.

While not the focus on this study, it is important to recognize that bone similarly grows radially in response to mechanical loading (reviewed by Frost [1]), with shear stress being the primary modality of mechanosensation at the cellular level (reviewed by Bonewald [2]). In bone as in arteries, shear stress elicits induction of *Nos3* [7]. Indeed, it was on the basis of the clinically important mechanical differences found in bone in the HcB-8 and HcB-23 strains, and our prior results suggesting that differences in ECE1 activity and expression are critical to these differences, that motivated the current work. The proposed relationships outlined in Fig. 6 are not only consistent with the literature in arteries but also in bone and may represent a master-controller for mechanosensitivity. However, this suggestion must await confirmation with future, mechanistic studies.

This work is the first to report blood pressure and vascular phenotypes in HcB-8 and HcB-23 mice. While these findings are intriguing, there are some important limitations. First, our data suggest a regulatory mechanism for arterial modeling through the endothelin pathway but they do not demonstrate a cause-and-effect relationship. While the two genotypes differ in the chromosome 4 segment harboring *Ece1*, they also harbor different alleles

over several other genomic regions. Second, the hemodynamic studies were conducted before we obtained the ambulatory BP data, and we did not measure cardiac chamber dimensions or wall thicknesses. Third, the experiments reported here are limited to young, skeletally mature animals. As our data suggest that older HcB-8 animals may be at risk of developing atherosclerosis and/or heart failure as a result of hypertension, an important future study would focus on older animals of these genotypes. Fourth, the isolated vessel mechanical tests were performed with identical axial stretch ratios (∼1.5) whereas in fact the HcB-8 carotids are under more axial stretch (∼2.0) *in vivo*. This should lead to somewhat more compliance in the HcB-8 carotids and reduce the differences in compliance found here. However, we expect the higher compliance of the HcB-23 mice to persist *in vivo*, due to their lower BP.

Conclusion

These experiments provide evidence that bones and arteries may share a common regulatory mechanism, resulting in parallel, genetically-mediated differences in arterial and long bone structure. Genetically induced high expression of *Ece1* is correlated with large diameter bones and arteries, low BP, low heart weight, and high *Nos3* expression in the myocardium and endothelium. These findings strongly indicate *Ece1*'s status as a candidate gene for the chromosome 4 bone QTL and suggest that its pleiotropy also mediates differences in BP and vascular structure. Differences in the localization of endothelin signaling, mediated by *Ece1* expression, may represent a potential mechanism that contributes to the epidemiological association between atherosclerotic disease and osteoporosis.

Acknowledgment

This work was supported by the ORDBL, R&D Service, Department of Veterans Affairs (RDB), National Institutes of Health Grant Nos. HL086939 (NCC), AR054753 (RDB), and AHA 10POST2640148 (ZW). Some of the work was conducted in the Madison VA Geriatrics Research, Education, and Clinical Center. This report is Madison GRECC manuscript 10-22.

We gratefully acknowledge Dr. Peter Demant for the gift of HcB-8 and HcB-23 mice, Dr. Theodore Goodfriend for critical review of the manuscript, and Dr. Timothy Hacker and Larry Whitesell for their surgical expertise.

References

[1] Frost, H. M., 2001, "From Wolff's Law to the Utah Paradigm: Insights About Bone Physiology and Its Clinical Applications," Anat. Rec., **262**, pp. 398–419.
[2] Bonewald, L. F., 2006, "Mechanosensation and Transduction in Osteocytes," Bonekey Osteovis., **3**, pp. 7–15.
[3] Humphrey, J. D., 2008, "Mechanisms of Arterial Remodeling in Hypertension: Coupled Roles of Wall Shear and Intramural Stress," Hypertension, **52**, pp. 195–200.
[4] Fox, S. W., Chambers, T. J., and Chow, J. W., 1996, "Nitric Oxide is an Early Mediator of the Increase in Bone Formation by Mechanical Stimulation," Am. J. Physiol., **270**, pp. E955–E960.
[5] Balligand, J. L., Feron, O., and Dessy C., 2009, "eNOS Activation by Physical Forces: From Short-Term Regulation of Contraction to Chronic Remodeling of Cardiovascular Tissues," Physiol. Rev., **89**, pp. 481–534.
[6] Helfrich, M. H., Evans, D. E., Grabowski, P. S., Pollock, J. S., Ohshima, H., and Ralston, S. H., 1997, "Expression of Nitric Oxide Synthase Isoforms in Bone and Bone Cell Cultures," J. Bone Miner. Res., **12**, pp. 1108–1115.
[7] Klein-Nulend, J., Helfrich, M. H., Sterck, J. G., MacPherson, H., Joldersma, M., Ralston, S. H., Semeins, C. M., and Burger, E. H., 1998, "Nitric Oxide Response to Shear Stress by Human Bone Cell Cultures is Endothelial Nitric Oxide Synthase Dependent," Biochem. Biophys. Res. Commun., **250**, pp. 108–114.
[8] MacPherson, H., Noble, B. S., and Ralston, S. H., 1999, "Expression and Functional Role of Nitric Oxide Synthase Isoforms in Human Osteoblast-Like Cells," Bone, **24**, pp. 179–185.
[9] Tanko, L. B., Christiansen, C., Cox, D. A., Geiger, M. J., McNabb, M. A., and Cummings, S. R., 2005, "Relationship Between Osteoporosis and Cardiovascular Disease in Postmenopausal Women," J. Bone Miner. Res., **20**, pp. 1912–1920.
[10] Ness, J., and Aronow, W. S., 2006, "Comparison of Prevalence of Atherosclerotic Vascular Disease in Postmenopausal Women With Osteoporosis or Osteopenia Versus Without Osteoporosis or Osteopenia," Am. J. Cardiol., **97**, pp. 1427–1428.
[11] Sennerby, U., Melhus, H., Gedeborg, R., Byberg, L., Garmo, H., Ahlbom, A., Pedersen, N. L., and Michaëlsson, K., 2009, "Cardiovascular Diseases and Risk of Hip Fracture," JAMA, **302**, pp. 1666–1673.
[12] Bagger, Y. Z., Rasmussen, H. B., Alexandersen, P., Werge, T., Christiansen, C., and Tankó, L. B., 2007, "Links Between Cardiovascular Disease and Osteoporosis in Postmenopausal Women: Serum Lipids or Atherosclerosis Per Se?," Osteoporos. Int., **18**, pp. 505–512.
[13] Sattler, A. M., Schoppet, M., Schaefer, J. R., and Hofbauer, L. C., 2004, "Novel Aspects on RANK Ligand and Osteoprotegerin in Osteoporosis and Vascular Disease," Calcif. Tissue Int. **74**, pp. 103–106.
[14] Groot, P. C., Moen, C. J., Dietrich, W., Stoye, J. P., Lander, E. S., and Demant, P., 1992, "The Recombinant Congenic Strains for Analysis of Multigenic Traits: Genetic Composition," FASEB J., **6**, pp. 2826–2835.
[15] Saless, N., Litscher, S. J., Lopez Franco, G. E., Houlihan, M. J., Sudhakaran, S., Raheem K. A., O'Neil, T. K., Vanderby, R., Demant, P., and Blank, R. D., 2009, "Quantitative Trait Loci for Biomechanical Performance and Femoral Geometry in an Intercross of Recombinant Congenic Mice: Restriction of the Bmd7 Candidate Interval," FASEB J., **23**, pp. 2142–2154.
[16] Saless, N., Lopez Franco, G. E., Litscher, S., Kattappuram, R. S., Houlihan, M. J., Vanderby, R., Demant, P., and Blank, R. D., 2010, "Linkage Mapping of Femoral Material Properties in a Reciprocal Intercross of HcB-8 and HcB-23 Recombinant Mouse Strains," Bone, **46**, pp. 1251–1259.
[17] Saless, N., Litscher, S. J., Houlihan, M. J., Han, I. K., Wilson, D., Demant, P., and Blank, R. D., 2011, "Comprehensive Skeletal Phenotyping and Linkage Mapping in an Intercross of Recombinant Congenic Mouse Strains HcB-8 and HcB-23," Cells Tissues Organs, **194**, pp. 244–248.
[18] Saless, N., Litscher, S. J., Vanderby, R., Demant, P., and Blank, R. D., 2011, "Linkage Mapping of Principal Components for Femoral Biomechanical Performance in a Reciprocal HCB-8 *x* HCB-23 Intercross," Bone, **48**, pp. 647–653.
[19] Xu, D., Emoto, N., Giaid, A., Slaughter, C., Kaw, S., de Wit, D., and Yanagisawa, M., 1994, "ECE-1: A Membrane-Bound Metalloprotease that Catalyzes the Proteolytic Activation of Big Endothelin-1," Cell, **78**, pp. 473–485.
[20] Gray, G. A., and Webb, D. J., 1996, "The Endothelin System and its Potential as a Therapeutic Target in Cardiovascular Disease," Pharmacol. Ther., **72**, pp. 109–148.
[21] Marsen, T. A., Egink, G., Suckau, G., and Baldamus, C. A., 1999, "Tyrosine-Kinase-Dependent Regulation of the Nitric Oxide Synthase Gene by Endothelin-1 in Human Endothelial Cells," Pflugers Arch., **438**, pp. 538–544.
[22] Herrera, M., and Garvin, J. L., 2004, "Endothelin Stimulates Endothelial Nitric Oxide Synthase Expression in the Thick Ascending Limb," Am. J. Physiol. Renal Physiol., **287**, pp. F231–F235.
[23] Ooi, C. Y., Wang, Z., Tabima, D. M., Eickhoff, J. C., and Chesler, N. C., 2010, "The Role of Collagen in Extralobar Pulmonary Artery Stiffening in Response to Hypoxia-Induced Pulmonary Hypertension," Am. J. Physiol. Heart Circ. Physiol., **299**, pp. H1823–H1831.
[24] Fung, Y. C., and Liu, S. Q., 1991, "Changes of Zero-Stress State of Rat Pulmonary Arteries in Hypoxic Hypertension," J. Appl. Physiol., **70**, pp. 2455–2470.
[25] Lemma, M., Innorta, A., Pettinari, M., Mangini, A., Gelpi, G., Piccaluga, M., Danna, P., and Antona, C., 2006, "Flow Dynamics and Wall Shear Stress in the Left Internal Thoracic Artery: Composite Arterial Graft Versus Single Graft," Eur. J. Cardiothorac. Surg., **29**, pp. 473–478.
[26] Peterson, L. H., Jensen, R. E., and Parnell, J., 1960, "Mechanical Properties of Arteries *In Vivo*," Circ. Res., **8**, pp. 622–639.
[27] Kobs, R. W., Muvarak, N. E., Eickhoff, J. C., and Chesler, N. C., 2005, "Linked Mechanical and Biological Aspects of Remodeling in Mouse Pulmonary Arteries With Hypoxia-Induced Hypertension," Am. J. Physiol. Heart Circ. Physiol., **288**, pp. H1209–H1217.
[28] Kobs, R. W., and Chesler, N. C., 2006, "The Mechanobiology of Pulmonary Vascular Remodeling in the Congenital Absence of eNOS," Biomech. Model. Mechanobiol., **5**, pp. 217–225.
[29] Zhao, J., Day, J., Yuan, Z. F., Gregersen, H., 2002, "Regional Arterial Stress-Strain Distributions Referenced to the Zero-Stress State in the Rat," Am. J. Physiol. Heart Circ. Physiol., **282**, pp. H622–H629.
[30] Edwards, C. A., and O'Brien, W. D., Jr., 1980, "Modified Assay for Determination of Hydroxyproline in a Tissue Hydrolyzate," Clin. Chim. Acta, **104**, pp. 161–167.
[31] Barger, J. L., Kayo, T., Pugh, T. D., Prolla, T. A., and Weindruch, R., 2008, "Short-Term Consumption of a Resveratrol-Containing Nutraceutical Mixture Mimics Gene Expression of Long-Term Caloric Restriction in Mouse Heart," Exp. Gerontol., **43**, pp. 859–866.
[32] Turner, C. H., and Burr, D. B., 1993, "Basic Biomechanical Measurements of Bone: A Tutorial," Bone, **14**, pp. 595–608.
[33] Lucitti, J. L., Jones, E. A., Huang, C., Chen, J., Fraser, S. E., and Dickinson, M. E., 2007, "Vascular Remodeling of the Mouse Yolk Sac Requires Hemodynamic Force," Development, **134**, pp. 3317–3326.
[34] Hall, C. E., Hurtado, R., Hewett, K. W., Shulimovich, M., Poma, C. P., Reckova, M., Justus, C., Pennisi, D. J., Tobita, K., Sedmera, D., Gourdie, R. G., and Mikawa, T., 2004, "Hemodynamic-Dependent Patterning of Endothelin Converting Enzyme 1 Expression and Differentiation of Impulse-Conducting Purkinje Fibers in the Embryonic Heart," Development, **131**, pp. 581–592.
[35] Sedmera, D., Harris, B. S., Grant, E., Zhang, N., Jourdan, J., Kurkova, D., and Gourdie, R. G., 2008, "Cardiac Expression Patterns of Endothelin-Converting

Enzyme (ECE): Implications for Conduction System Development," Dev. Dyn., **237**, pp. 1746–1753.
[36] Takebayashi-Suzuki, K., Yanagisawa, M., Gourdie, R. G., Kanzawa, N., and Mikawa, T., 2000, "*In Vivo* Induction of Cardiac Purkinje Fiber Differentiation by Coexpression of Preproendothelin-1 and Endothelin Converting Enzyme-1," Development, **127**, pp. 3523–3532.
[37] Tuttle, J. L., Nachreiner, R. D., Bhuller, A. S., Condict, K. W., Connors, B. A., Herring, B. P., Dalsing, M. C., and Unthank, J. L., 2001, "Shear Level Influences Resistance Artery Remodeling: Wall Dimensions, Cell Density, and eNOS Expression," Am. J. Physiol. Heart Circ. Physiol., **281**, pp. H1380–H1389.
[38] Korshunov, V. A., and Berk, B. C., 2004, "Strain-Dependent Vascular Remodeling: The 'Glagov Phenomenon' is Genetically Determined," Circulation, **110**, pp. 220–226.
[39] Mawji, I. A., and Marsden, P. A., 2003, "Perturbations in Paracrine Control of the Circulation: Role of the Endothelial-Derived Vasomediators, Endothelin-1 and Nitric Oxide," Microsc. Res. Tech., **60**, pp. 46–58.